Contribution of integration the TCSC device and wind farms on power system

ADJOUDJ LABIBA[1], LAKDJA FATIHA[2], GHERBI FATIMA ZOHRA[1]
[1]Engineering Department. Intelligent Control and Electrical Power System Laboratory (ICEPS)
[2]The Department of Electrical Engineering, Saida University, Engineering Department. Intelligent Control and Electrical Power System Laboratory (ICEPS)
Djillali Liabes University, Sidi bel Abbes, 22000
ALGERIA
Adjoudj-l@hotmail.fr, flakdja@yahoo.fr , fzgherbi@gmail.com

Abstract: - Generation of electricity from wind power has received considerable attention and integration of wind farms based on double fed induction generators (DFIG) may have significant impacts on power system operation. This paper analyzes and compares the integrating of wind farm and Flexible AC Transmission System devices (FACTS) and their impact on IEEE-9 bus and IEEE-30 bus test systems. The west-Algerian network (2012) is also selected for study and different cases have been simulated in MATLAB based Power System Analysis Toolbox. Therefore, we must choose among FACTS devices, those with specific applications such as controlling the power flow, Thyristor-controlled series compensator (TCSC) is the best choice for a proper control of power flow and consequently the reduction of active and reactive power losses. The simulation results show clearly the effect of wind farm and TCSC device on power quality of electric power system.

Key-Words: - Power System - TCSC - wind power generation – DFIG - power flow analysis – Power System Analysis Toolbox.

1 Introduction

As a clean, renewable energy, wind power has been a common concern recently all over the world. The world's newly installed capacity of wind power was 38.31 million kilowatts in 2009, and the total installed capacity reached 157.9 million kilowatts [1]. The development of production technology is improving the wind turbine performance. As a result of these developments, and the measures to promote the construction of renewable resources, more utilities are seriously examining the wind option [2]. With the development of wind power and the increasing of wind farm capacity, the interaction between wind farms and power system has become increasingly evident [3]. Due to the increasing concern about CO2 emissions, renewable energy systems and especially wind energy generation have attracted great interests in recent years [4]. Making full use of wind energy to generate electricity can not only reduce the environmental pollution but also reduce the fuel cost of the power system [5]. Nowadays, as a consequence of the important progress in power electronics and micro-computing, the control of AC electric machines has seen considerable development and the possibility for application [6]. Doubly Fed Induction Generator (DFIG) is a kind of variable speed constant frequency wind generator which can output reactive power when not working in the constant power factor mode and be used as a reactive power supply for wind farm [7]. DFIG is one of the most commonly used technologies nowadays, as these offer advantages such as the decoupled control of active and reactive powers [8]. DFIG has higher energy capture efficiency and improved power quality. With the advent of power electronics, a back-to-back converter, which consists of two bidirectional converters and a dc-link acts as an optimal operation tracking interface between generator and the grid [9]. DFIGs have two operation modes which are constant-power factor and constant-voltage control. The essential differences between them are different reactive power dispatch and voltage control strategies. Thus the study on operation modes of DFIG has a great significance for improving system voltage stability [10]. Flexible AC Transmission System

(FACTS) controller is defined as power electronic based system and other static equipment that provide control of one or more AC transmission system parameters [11]. FACTS have been introduced in 1980's and used as economical and efficient means to control the power transfer in an interconnected AC transmission system [12]. From the 1990s, with the concept of FACTS devices introduced by Prof. N.G.Hingorani, the complexity in power flow control vanishes slowly [13]. The objective of FACTS devices is to bring a system under control and to transmit power as ordered by the control centers, it also allows increasing the usable transmission capacity to its maximum thermal limits [14]. FACTS devices can be used for voltage stability and reactive power compensations, controlling the power flow [15]. By Using FACTS devices it is possible to control the phase angle, the voltage magnitude at chosen buses and /or line impedances of a transmission system [14]. Thyristor controlled series compensator (TCSC) is one of the important members of FACTS family that is increasingly applied by the utilities in modern power systems with long transmission lines [16]. Thyristor Controlled Series Capacitor (TCSC) is one of the series connected FACTS device that increase power transfer capability of long lines and voltage stability [17]. TCSC has various roles in the operation and control of power systems, such as scheduling power flow; reducing net loss; providing voltage support; limiting short circuit currents; mitigating sub-synchronous resonance (SSR); damping the power oscillations; and enhancing transient stability [18,19]. The power system stability enhancement via PSS and a thyristor controlled series capacitor (TCSC)- based stabilizer when applied independently and also through coordinated application was discussed and investigated in [20,21]. TCSC is inserted into a transmission line to vary its reactance, and thereby reduce the reactive losses and increase the transmission capacity [22]. The transmitted power through a line is inversely proportional to the transfer impedance [23]. The TCSC has a great application and ability of exactly adjusting the power flow on a transmission line [24]. TCSC offers smooth and flexible control of the branch impedance with much faster response [25]. The TCSC's high speed switching capability provides a mechanism for controlling line power flow, which permits increased loading of existing transmission lines, and allows for rapid readjustment of line power flow in response to various contingencies.

The TCSC also can regulate steady-state power flow within its rating limits [26]. The implementation of FACTS is fast and the capital investments are reduced compared to other solutions (construction of new transmission lines or new means of production) [27]. This work describes a study on the insertion of TCSC and wind farm on IEEE-9 bus and IEEE-30 bus test systems and investigates the application of the proposed approach on real network data. The west-Algerian network 2012 (400kV, 220kV and 60kV) is selected for study and different cases have been simulated in a powerful tool for simulation which is the Power System Analysis Toolbox (PSAT). PSAT is a MATLAB toolbox for electric power system analysis and the control was designed by Vanfretti and Milano [28]. The main purpose of this paper is to enhance the power flow and resolve the voltage instability.

2 Modeling of components

2.1 Thyristor-controlled series compensator (TCSC)

TCSC vary the electrical length of the compensated transmission line which enables it to be used to provide fast active power flow regulation. It also increases the stability margin of the system. The simpler TCSC model exploits the concept of a variable series reactance. The series reactance is adjusted automatically, within limits, to satisfy a specified amount of active power flow through it [29]. The model of the TCSC used in this paper is a variable reactance connected in series with transmission line [30] that is:

$$Z_k = r_k + j(x_k + x_{TCSC}),\ \forall\, k=(n,m) \in \Omega_{TCSC} \quad (1)$$

The resulting conductance and susceptance are, respectively:

$$g_k = \frac{r_k}{r_k^2 + (x_{k+} x_{TCSC})^2}, \forall k = (n,m) \in \Omega_{TCSC} \quad (2)$$

$$b_k = \frac{-(x_{k+} x_{TCSC})}{r_k^2 + (x_k + x_{TCSC})^2}, \forall\ k = (n,m) \in \Omega_{TCSC} \quad (3)$$

Where Z_k : Impedance of element k; r_k : Resistance of element k; x_k : Reactance of element k; x_{TCSC} : Maximum reactance of the TCSC; g_k : Conductance of element k; b_k : Series susceptance

of element k; Ω_{TCSC}: set of lines with TCSCs. The TCSC is composed of an inductance x_L in series with a thyristor dimmer; all in parallel with a capacitor x_c, the equivalent susceptance B of the TCSC is function of the firing angle α, the inductance x_L and the capacitor x_c [27]. TCSC regulator is depicted in Figure 2. The system undergoes the algebraic equations:

$$P_{km} = V_k V_m (Y_{km} + B)\sin(\theta_k - \theta_m) \quad (4)$$

$$P_{mk} = -P_{km} \quad (5)$$

$$Q_{km} = V_k^2 (Y_{km} + B) - V_k V_m (Y_{km} + B)\cos(\theta_k - \theta_m) \quad (6)$$

$$Q_{mk} = V_m^2 (Y_{km} + B) - V_k V_m (Y_{km} + B)\cos(\theta_k - \theta_m) \quad (7)$$

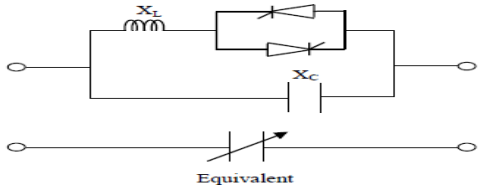

Fig.1 Simple diagram of TCSC

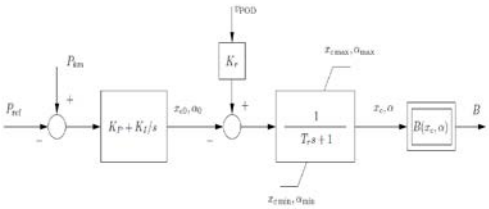

Fig.2 TCSC regulator.

Where the indexes *k* and *m* stand for the sending and receiving bus indices, respectively, Y_{km} is the admittance, *P* and *Q* are the active and reactive power of the line at which the TCSC is connected respectively. V_k and V_m are the voltage magnitude at bus *k* and *m* respectively. The TCSC differential equations are as follows:

$$\dot{X}_1 = (\{x_{co}, \alpha_0\} + K_r u_{POD} - x_1)/T_r \quad (8)$$

Where x_1 is state variable, x_{co} is the initial series reactance, α_0 is the initial firing angle, K_r is the gain of the stabilizing signal, u_{POD} is connection status and T_r is the regulator time constant.

$$\dot{X}_2 = K_I (P_{km} - P_{ref}) \quad (9)$$

x_2 is state variables, K_I is the Integral gain of PI controller and P_{ref} is the reference power flow of the PI controller.

$$\{x_{co}, \alpha_0\} = K_p (P_{km} - P_{ref}) + x_2 \quad (10)$$

K_p is the proportional gain of PI controller.

The state variable $x_1 = \{x_c, \alpha_0\}$, depending on the TCSC model.

The PI controller is enabled only for the constant power flow operation mode. The output signal is the series susceptance *B* of the TCSC and it is depending on the TCSC model $B(x_c)$ or $B(\alpha)$. During the power flow analysis the TCSC is modeled as a constant capacitive reactance that modifies the line reactance x_{km}, as follows:

$$x'_{km} = (1 - c_p) x_{km} \quad (11)$$

Where c_p is the percentage of series compensation. The TCSC state variables are initaliazed after the power flow analysis as well as the reference power of the PI controller P_{ref}. At this step, a check of x_c and/or α anti-windup limits is performed [31].

2.2 Double fed induction generator (DFIG) model

The overall scheme for a wind farm based on DFIG is depicted in Figure 3. Thus; it is composed by two voltage fed PWM converters in back-to-back configuration. These converters allow the decoupled control of the active and reactive power flow between the DFIG and the AC network by adjusting the switching of the IGBTs.

For this structure, the equations of the double feed induction generator in terms of the d and q axes and neglecting the stator and rotor flux transients can be written as [8][32].

For the stator circuit:

$$v_{ds} = -R_s i_{ds} + (x_s + x_m) i_{qs} + x_m i_{qr} \quad (12)$$

$$v_{qs} = -R_s i_{qs} - (x_s + x_m) i_{ds} + x_m i_{dr} \quad (13)$$

For the rotor circuit:

$$v_{dr} = -R_r i_{dr} + (1 - \omega)((x_r + x_m) i_{qr} + x_m i_{qs} \quad (14)$$

$$v_{qr} = -R_r i_{qr} + (1 - \omega)((x_r + x_m) i_{dr} + x_m i_{ds} \quad (15)$$

Where v_{ds}, v_{qs}: d and q axes stator voltages; v_{dr}, v_{qr}:d and q axes rotor voltages; i_{ds}, i_{qs}: d and q axes stator currents; i_{dr}, i_{qr} d and q axes rotor currents; R_s, R_r: Stator and rotor resistances; x_s: Stator self-reactance; x_r: Rotor self-reactance; x_m: Mutual reactance; ω: Rotor speed. Assuming a lossless converter model, active power of the converter coincides with the rotor active power.

The reactive power injected into the grid can be approximated neglecting stator resistance and assuming that the d- axis coincides with the maximum of the stator flux. Therefore, the powers injected in the grid result [31]:

$$P = v_{ds} i_{ds} + v_{qs} i_{qs} + v_{dr} i_{dr} + v_{qr} i_{qr} \quad (16)$$

$$Q = -\frac{x_m v i_{dr}}{x_s + x_m} - \frac{v^2}{x_m} \quad (17)$$

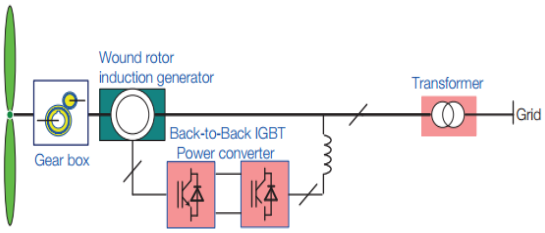

Fig.3 Doubly feed induction generator.

Where v is the grid voltage magnitude. The mechanical torque of the Wind turbine model T_m is calculated using the given wind velocity V_w (m/s) as [33]:

$$T_m = \frac{p_w}{\omega} \quad (18)$$

$$p_w = \frac{1}{2}\rho c_p A V_w^3 \quad (19)$$

Where: ω is the rotor speed, Pw the mechanical power extracted from the wind, ρ is the air density (kg/m^2), c_p is the power coefficient and A is the rotor area (m^2).

Thus the electrical torque T_e and the mathematical link between T_m and T_e where H is the rotor inertia results:

$$T_e = x_m(i_{qr} i_{ds} - i_{dr} i_{qs}) \quad (20)$$

$$\frac{d\omega}{dt} = \frac{1}{2H}(T_m - T_e) \quad (21)$$

In order to model the instantaneous wind speed V_w *(t)*, it is assumed to be composed of four components as follows: Average and initial wind speed V_{wa} *(m/s);* ramp component of the wind speed V_{wr} *(t)*; gust component of the wind speed V_{wg} *(t)* and wind speed turbulence V_{wt} *(t)* [34]. Thus the resulting wind speed V_w *(t)* is:

$$V_w(t) = V_{wa} + V_{wr}(t) + V_{wg}(t) + V_{wt}(t) \quad (22)$$

The wind ramp component is defined by amplitude A_{wr} and starting and ending times, t_{sr} and t_{er} respectively:

$$t < t_{sr} : V_{wr}(t) = 0$$

$$t_{sr} \le t \le t_{er} : V_{wr}(t) = A_{wr} \frac{(t - t_{sr})}{(t_{er} - t_{sr})} \quad (23)$$

$$t > t_{er} : V_{wr}(t) = A_{wr}$$

The wind gust component is defined by amplitude A_{wg} and starting and ending times, t_{sg} and t_{eg} respectively:

$$t < t_{sg} : V_{wg}(t) = 0$$

$$t_{sg} \le t \le t_{eg} : V_{wg}(t) = \frac{A_{wg}}{2}\left(1 - \cos\left(2\pi \frac{t - t_{sg}}{t_{eg} - t_{sg}}\right)\right) \quad (24)$$

$$t > t_{eg} : V_{wg}(t) = A_{wg}$$

The wind turbulence component is described by a power spectral density as follows [31]:

$$S_{wt} = \frac{\frac{1}{(\ln(\frac{h}{z_0}))^2} \times l V_{wa}}{(1 + 1.5\frac{lf}{V_{wa}})^{\frac{5}{3}}} \quad (25)$$

Where f is the electrical frequency, h (meters) the wind turbine tower height, l (meters) is the turbulence length scale (= 20 h for h < 30 meters, and 600 meters for h > 30 meters), z_0 (meters) is the roughness length. The spectral density is then converted in a time domain cosine series [31].

$$V_{wt}(t) = \sum_{i=1}^{n} \sqrt{S_{wt}(f_i)\Delta f}\cos(2\pi f_i t + \varphi_i + \Delta\varphi) \quad (26)$$

Where f_i and φ_i are the frequency and the initial phase of the *ith* frequency component, being φ_i

random phases ($\varphi_i \in [0, 2\pi]$). The frequency step Δf should be $\Delta f \in (0.1, 0.3)$ Hz. Finally $\Delta\varphi$ is a small random phase angle introduced to avoid periodicity of the turbulence signal.

3 Results and discussion

In this paper different studies are selected to increase the power flow and to get better power quality of the system. To compare the impact of wind farm and TCSC on IEEE-9 bus and IEEE-30 bus test systems, simulation cases can be applied in PSAT 2.1.8 by using Newton-Raphson method. The TCSC control powers in the transmission lines in order to minimize power losses, the index used in this study for the optimal location of the TCSC, is to determine the most line causes significant active losses in the systems. Parameters of TCSC device used in simulation are presented in Table 1.

Wind farm of 600 MVA / 69kV capacity comprising of 300 wind turbines has been connected to most critical bus by creating another bus through a transformer of tap ratio unity. Wind was modeled as Weibull distribution as proposed by Milano. F (2005) by taking into account the composite nature of wind which included average, ramp, gust, turbulence and low pass filters were used to smooth the wind speed variations[34]. Parameters of DFIG and Wind model are given in Table 2.

Table 1. TCSC parameters.

Sn	Power rating	100 MVA
Cp	Percentage of series compensation	40 %
Tr	Regulator time constant	1 s
X_{Cmax}	Maximum reactance	0.5 p.u.
X_{Cmin}	Minimum reactance	-0.5 p.u.
KP	Proportional gain of PI controller	5 p.u./p.u.
K_I	Integral gain of PI controller	1 p.u./p.u.
X_L	Reactance (inductive)	0.2 p.u.
X_C	Reactance (capacitive)	0.1 p.u.
Kr	Gain of the stabilizing signal	10 p.u./p.u.

3.1 Study on IEEE-9 bus test system

The IEEE 9 Bus Test represents a portion of the Western System Coordinating Council (WSCC) 3-Machines 9-Bus system. Basically, this 9 bus system contains 3 generators, 9 buses and 3 load and the base KV levels in the go from 16.5 kV to 230 kV, System load is 315 MW and 115 Mvar [35]. Figure 4 shows IEEE 9 bus test system with wind farm and TCSC device inserted in PSAT.

To determine the optimal emplacement of TCSC device, the power flow simulation is a necessary step to determine the most line causes significant active losses, line 4 between (buses 7 bus 5) with a value of 2.299 MW was chosen as an optimal position of TCSC. The series reactance x_{TCSC} is adjusted automatically and takes a value of 0.0644 p.u. The reference power flow of the PI controller is 0.95342 p.u.

Table 2. DFIG parameters for IEEE bus test systems.

Power, Voltage and Frequency Ratings [MVA, kV, Hz]	[600, 69, 60]
Stator Resistance Rs, stator Reactance Xs [p.u, p.u.]	[0.01, 0.10]
Rotor Resistance Rr, Rotor Reactance Xr [p.u, p.u.]	[0.01, 0.08]
Magnetization Reactance Xm [p.u.]	[3.00]
Pitch control gain Kp, time constant Tp [p.u,s]	[10, 3]
Voltage control gain Kv, Power Control time constant Te [p.u, s]	[10, 0.01]
Number of Pole, gear box ratio [int, -]	[4, 1/89]
Blade length, number [m, int]	[75.00, 3]
P_{max} and P_{min} [p.u, p.u.]	[1.00, 0.00]
Q_{max} and Q_{min} [p.u, p.u.]	[0.7, -0.7]
Number of generators	300
Nominal wind speed, air density [m/s, kg/m3]	[15, 1.225]
Filter time constant, sample time [s, s]	[4, 0.1]
Weibull constant C and K	[20, 2]
Ramp constants tsr, ter and Awr [s, s, m/s]	[5, 15, 1]
Gust constants tsg, teg and Awg [s, s, m/s]	[5, 15, 0]
Turbulence constants h, Z0, Δf and n [m, -, Hz, -]	[50, 0.01, 0.2, 50]

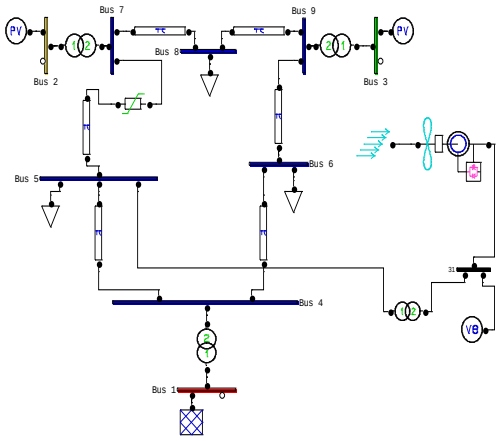

Fig.4 IEEE 9 bus system inserted in PSAT with wind farm and TCSC device.

After the insertion of TCSC device in the system, the active losses of line 4 decrease by 2.299 MW to 0 MW, line 2 decreases by 0.4752 MW to 0.38031MW, the same for line 3 by 1.35384MW to 0.9998 MW, and line 5 by 0.25751MW to 0.181865MW. Figure 6 shows the active losses of IEEE-9 bus test system with and without TCSC device.

The power flow simulation shows the most suitable and critical voltage bus in the system. Wind farm has been connected to bus 5 with low voltage value of 0.99563 p.u by creating a transformer with Primary and secondary voltage ratio (69 kV/230 kV).

From the results, wind farm injected 21.2202 MW and 0.4748 MVar. Figure 5 presents the wind speed of DFIG (m/s). The algebraic variables like the voltage reference of DFIG take value of 1.0003271 p.u, the rotor speed ω =0.43707784 p.u, the mechanical power extracted from the wind *Pw* =0.21220295 p.u and the static variable like V_w take value of 0.43707784 p.u.

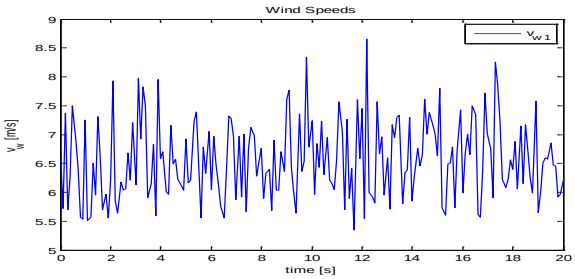

Fig.5 Wind speed of DFIG (m/s).

From the results as shown in Figure 6, wind farm decrease the active losses of line 4 by 2.2999 MW to 2.1544 MW, of line 5 by 0.2575 MW to 0.1418 MW and line 6 by 0.1664 MW to 0.1440 MW.

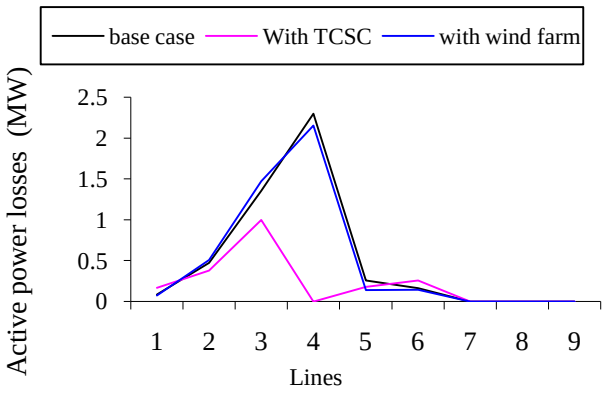

Fig.6 Active power losses of IEEE-9 bus test system in different cases.

Figure 7 shows that after the insertion of wind farm, the reactive power losses of line 4 decrease:
by -19.6935 MVar to -20.5086 MVar, the line 5 by -15.7941 MVar to -16.8209 MVar and line 9 by 3.1227 MVar to 1.7031 MVar.

Table 3 presents the line power flow of IEEE 9-bus test system of base case, system with TCSC and system with wind farm. After the insertion of TCSC in line 4 the reactive power flow of this line change from -8.3808 MVar to 19.7318 MVar and this increase justifies the growth of reactive losses in this line.

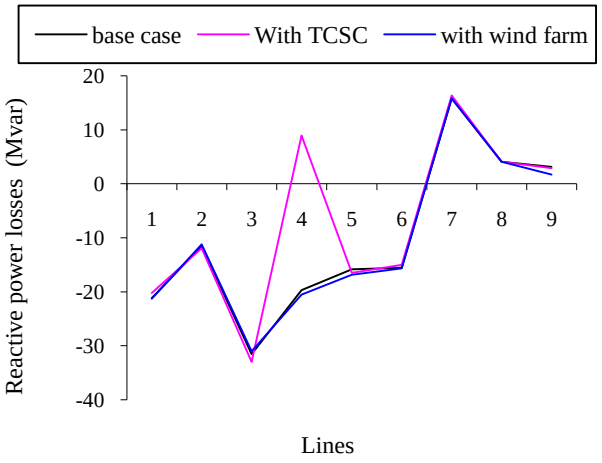

Fig.7 Reactive power losses of IEEE-9 bus test system in different cases.

Figure 8 shows the profile of voltage magnitude of IEEE-9 bus test system after the insertion of TCSC device and wind farm.

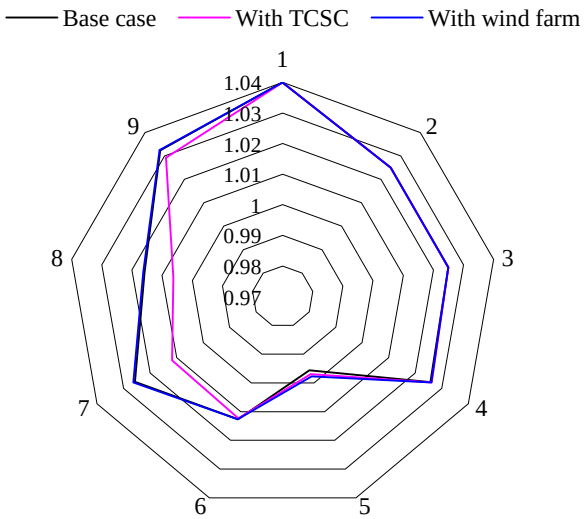

Fig.8 Voltage magnitude of IEEE-9 bus test system in different cases.

Table 3. Line power flow of IEEE 9 bus test system in different cases.

Cases			Base case		With TCSC		With Wind farm	
From Bus	To Bus	Line	P_{FLOW} (MW)	Q_{FLOW} (MVar)	P_{FLOW} (MW)	Q_{FLOW} (MVar)	P_{FLOW} (MW)	Q_{FLOW} (MVar)
Bus 9	Bus 8	1	24.183414	3.11951022	32.8891393	9.0483826	21.5137286	3.18407815
Bus 7	Bus 8	2	76.3798662	-0.79733307	67.6581544	-6.22924682	79.0695069	-0.71493367
Bus 9	Bus 6	3	60.816586	-18.0748373	52.1108607	-18.4880025	63.4862714	-18.3674937
Bus 7	Bus 5	4	86.6201338	-8.38082021	95.3418456	19.7318125	83.9304931	-9.28382852
Bus 5	Bus 4	5	-40.6798375	-38.6872517	-29.6581544	-39.2147217	-22.0486945	-39.2014257
Bus 6	Bus 4	6	-30.5372628	-16.5433668	-38.8889803	-15.5395302	-27.9884655	-17.3563325
Bus 2	Bus 7	7	163	6.65365602	163	29.8376555	163	5.82690877
Bus 3	Bus 9	8	85	-10.8597089	85	-5.39355498	85	-11.0850393
Bus 1	Bus 4	9	71.6410215	27.045928	68.9890533	26.1758548	50.3230922	25.7998096

3.2 Study on IEEE-30 bus test system

The 30 bus system has 34 transmission lines, 21 load buses, 6 generation buses and 2 fixed capacitors. System load is kept constant at 283.4 MW and 126.2 MVar with 100MVA base, 135 KV base and frequency as 60Hz [35]. Figure 9 shows IEEE 30 bus test system inserted in PSAT.

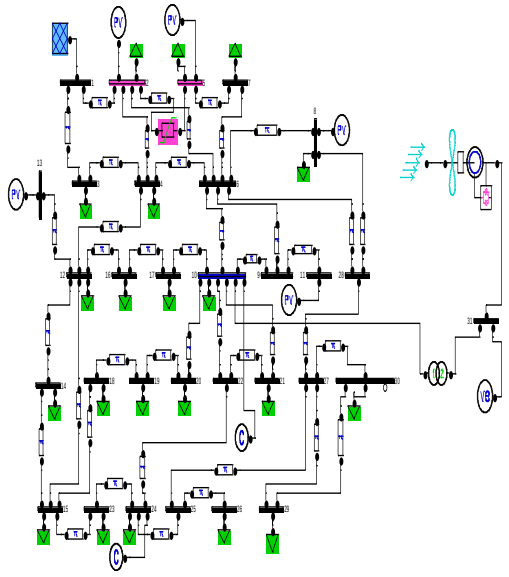

Fig.9. IEEE-30 bus test system with TCSC and wind farm inserted in PSAT.

The most line causes significant active losses and far from the production node is line 36 between (bus 2 and 5).

TCSC is connected to line 36 and x_{TCSC} is adjusted automatically with a value of 0.07932 p.u and reference power flow is 0.95314 p.u.

After the insertion of TCSC, the active losses of line 2 decrease by 3.11717 MW to 2.8223 MW, line 13 decrease by 1.001285 MW to 0.7739 MW, the same for line 32 by 0.38027 MW to 0.1274 MW, line 34 by 1.9489 MW to 1.5197 MW, line 36 by 2.9543 MW to 0 MW and line 37 by 0.8597 MW to 0.7759 MW. Figure 10 show this reduction in different lines of IEEE-30 bus test system.

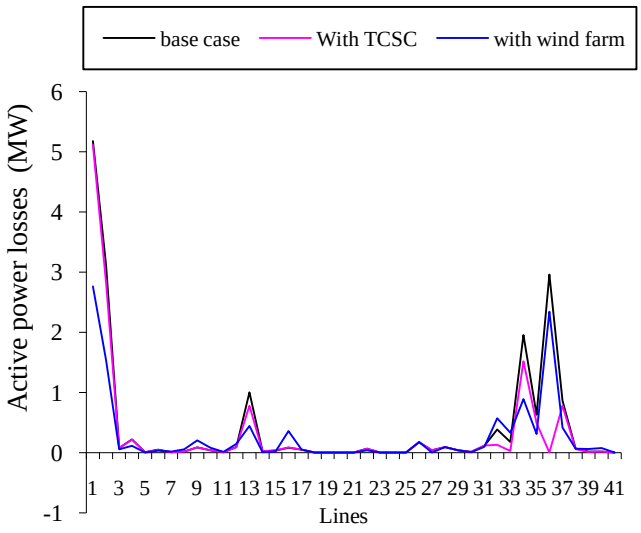

Fig.10 Active power losses of IEEE-30 bus test system in different cases.

Figure 11 show that TCSC device reduces the reactive power losses of line 2 by 9.1792 MVar to 8.10512 MVar, line 13 by 1.1035 MVar to 0.43256 MVar, line 32 by 0.3069 MVar to -0.4672 MVar and line 34 by 3.9427 MVar to 2.6502 MVar.

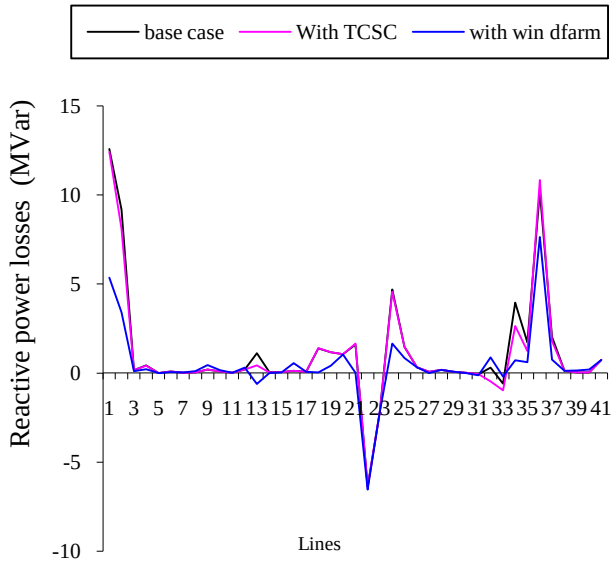

Fig.11 Reactive power losses of IEEE-30 bus test system in different cases.

For the IEEE 30 bus test system, the best choice for the insertion of wind farm is the compensation node 10 and its voltage value is 0.96406 pu. The active and reactive powers injected by wind farm are respectively 66.6760348 MW and 1.124227 MVar.

The wind farm reduces the active losses in line 1 by 5.1734 MW to 2.7632, line 13 by 1.00128 MW to 0.4407 MW, line 34 by 1.9489 MW to 0.8884 MW, line 36 by 2.9543 MW to 2.3425 MW and line 37 by 0.8597 MW to 0.4147 MW as shown in Figure 10.

After the integration of wind farm, the reactive power losses of line 1 decrease by 12.5757 MVar to 5.3562 MVar, line 2 by 9.1792 MVar to 3.4071 MVar, line 3 by 1.1035 MVar to -0.6161 MVar, line 18 by 1.3723 MVar to 0.0425 MVar, line 21 by 1.5984 MVar to 0.01838 MVar, line 24 by 4.6831 MVar to 1.66088 MVar, line 34 by 3.942731 MVar to 0.71495 MVar, line 36 by 10.210192 MVar to 7.63871 MVar and line 37 by 2.0322 MVar to 0.74995 MVar.

Figure 11 shows the impact of wind farm on reactive losses of IEEE-30 bus test system.

For better understand Figure 12 and 13 present respectively the impact of TCSC device and wind farm on active and reactive line power flow, Figure 14 show the voltage magnitude of nodes in different cases of IEEE-30 bus test system.

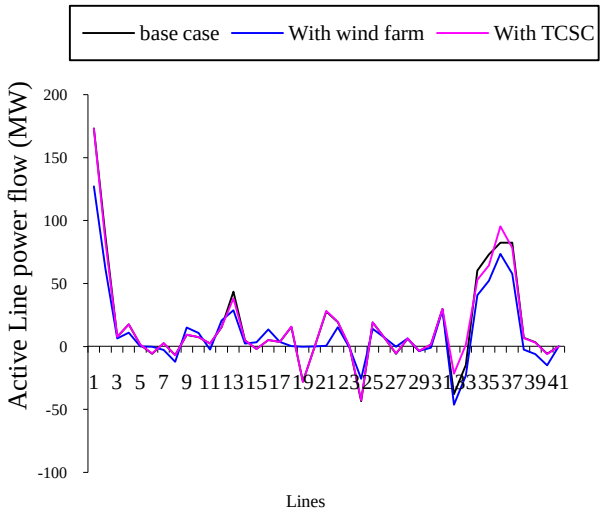

Fig.12 Active Power flow of IEEE-30 bus test system in different cases.

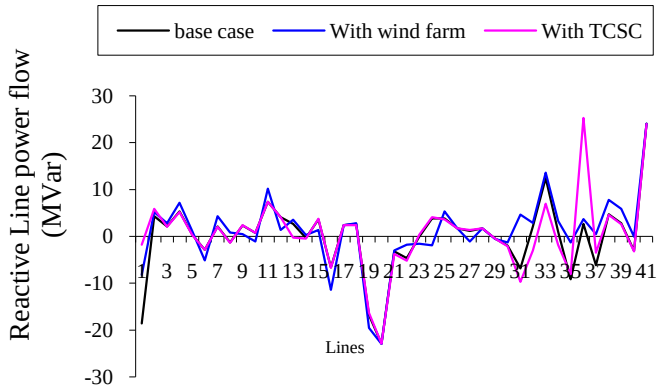

Fig.13 Reactive Power flow of IEEE-30 bus test system in different cases.

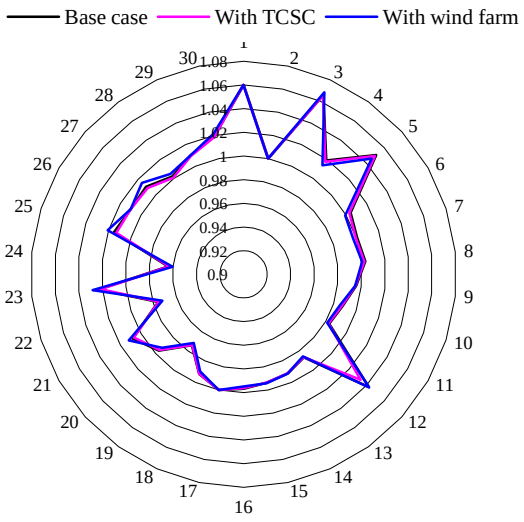

Fig.14 Voltage magnitude of IEEE-30 bus test system in different cases.

Table 4. Simulation results of IEEE-9 bus and IEEE-30 bus test systems in different cases.

IEEE-9 bus test system						
Cases	Total generation		Total losses		Slack bus generation	
	P_G(MW)	Q_G(MVar)	P_L(MW)	Q_L(MVar)	P_S(MW)	Q_S(MVar)
Base case	319.641	22.8399	4.641	-92.1601	71.641	27.0459
With TCSC	316.9891	50.62	1.9891	-64.38	68.9891	26.1759
With wind farm	319.5434	21.0165	4.5434	-93.9835	50.3231	25.7998
IEEE-30 bus test system						
Cases	Total generation		Total losses		Slack bus generation	
	P_G(MW)	Q_G(MVar)	P_L(MW)	Q_L(MVar)	P_S(MW)	Q_S(MVar)
Base case	301.014	172.5027	17.614	46.2427	261.014	-14.3798
With TCSC	296.4226	168.0928	13.0226	41.8328	256.4226	4.0527
With wind farm	295.2316	152.8488	11.8316	26.5888	188.5556	-3.0583

3.3 Application to the west Algerian network (2012)

The west-Algerian system 2012 (400 kV, 220 kV and 60 kV) is selected for study with 100MVA base and frequency as 50 Hz. System load is kept constant at 1686.24 MW and 664.67 Mvar. The system has 138 branches (lines and transformers), 102 buses,7 generation buses and 3 fixed capacitors.

Figure 17 represents the west Algerian network inserted in PSAT. According to the results of power flow, the most line causes significant losses is the line N°91 (bus 73-39). Bus 85 records the low voltage (0.7769 p.u), voltage magnitude of bus 73 is (0.78676 p.u) and this bus is indicated as the optimal position for wind farm connection. The wind farm of 600 MVA / 690 V capacity comprising of 300 wind turbines, frequency as 50 Hz, Stator resistance (Rs) as 0.00488 p.u, Stator leakage reactance (Xls) as 0.09241 p.u, Rotor resistance (Rr) as 0.00549 p.u, Rotor leakage reactance (Xlr) as 0.09955 p.u and Magnetizing reactance (Xm) as 3.95279 p.u.

Wind farm is connected to bus 73 by creating another bus through a transformer of tap ratio unity and wind was modeled as Weibull distribution as proposed by Milano. F (2005). The active and reactive powers injected by wind farm are respectively 48.1522 MW and 12.9803 MVar.

The TCSC device is connected to line 91 and takes a value of 0.04667 p.u. From the results the voltage magnitude of bus 73 increases after the insertion of TCSC device by 0.7867 p.u to 0.9235 p.u and increases after the insertion of wind farm to 0.9738 p.u. Figure 15 and 16 present respectively the active and reactive power losses of west Algerian network in different cases.

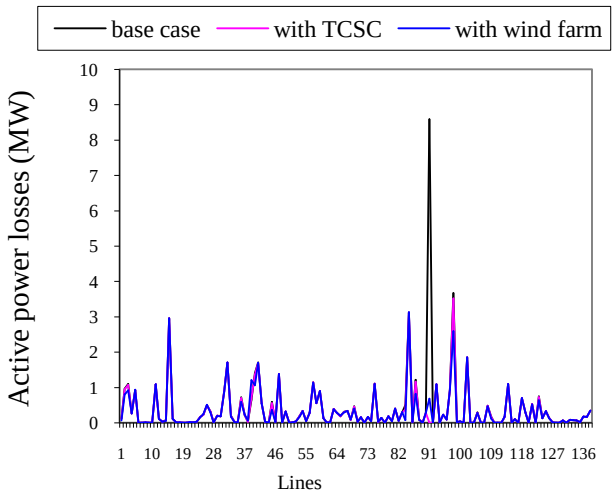

Fig.15 Active power losses of west Algerian network in different cases.

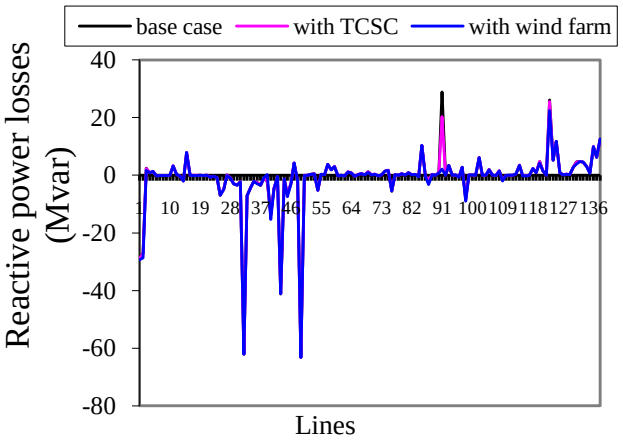

Fig.16 Reactive power losses of west Algerian network in different cases.

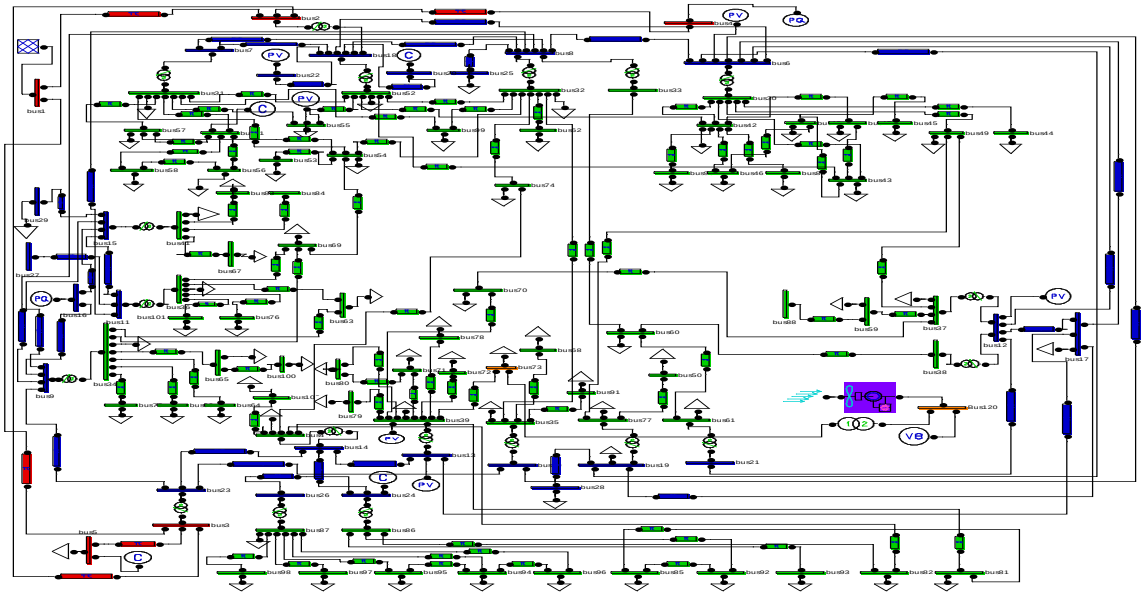

Fig.17 The west Algerian network inserted in PSAT.

Table 5. Simulation results of west Algerian network in different cases.

Simulation Cases	Total generation		Total losses		Slack bus Production	
	P_G(MW)	Q_G(MVar)	P_L(MW)	Q_L(MVar)	P_S(MW)	Q_S(MVar)
Base case	1742.5594	540.24321	56.3127	-124.4270	493.5594	-62.2165
With TCSC	1735.3925	530.5674	47.23448	-134.9949	486.3925	-61.8818
With wind farm	1734.0791	506.8012	45.91310	-158.7648	436.9279	-59.2654

After the integration of wind farm to the west Algerian network, the active power losses of line 2 decrease by 0.96 MW to 0.7991 MW, line 91 by 8.59 MW to 0.6823 MW and line 98 by 3.669 to 2.5894 MW. Wind farm reduces the reactive power losses of line 91 by 28.87 MVar to 2.091 MVar.

The TCSC device decrease the active power losses of line 2 by 0.96 MW to 0.94 MW, line 91 by 8.59 MW to 0 MW, line 98 by 3.669 MW to 3.5213 MW. The reactive power losses of line 91 decrease by 28.87 MVar to 20.307 MVar.

4 Conclusion

Simulation was illustrated by the use of one of the most recent software which is software PSAT. This last was applied without any failure or instability in simulation. The first part showed the positive contribution of the integration of TCSC device to the IEEE test systems on power transmitted. TCSC device is adjusted automatically, within limits, to satisfy a specified amount of active power flow through it. The second part devoted to the integration of wind farms, which has concluded that the use of wind farms has significant benefits in reducing generation and losses of real and reactive power in the systems according to the needs of the network. The proposed approach was also applied to west Algerian network and from the results presented in this paper it can conclude that the integration of wind turbine and TCSC enhances the power flow and resolve the problem of losses.

References:

[1] G. Li, B. Zhang, J. Wang, Z. Bo, T. Yip , D. Writer, L. Yu-ming . DFIG-based wind farm electromagnetic dynamic model and impact on protection relay of transmission network. *International Conference on Advanced Power System Automation and Protection (APAP);* 16-20 Oct 2011; Beijing, pp. 694-698.

[2] A. Gjukaj, R. Bualoti, M. Çelo, M. Kullolli. Wind Power Plant Data Monitorin and Evaluating. *Wseas transactions on power systems.* Vol.8, No.1,2013, pp. 24-34.

[3] A. Jiapaer, G. Zeng, S. Ma, H. Xie, Y. Tong, M. Huang. Study on Capacity of Wind Power Integrate into Power Grid Based on Static Voltage Stability. *15th International Conference*

on Harmonics and Quality of Power (ICHQP); 17-20 June 2012*;* Hong Kong , pp. 855-859.

[4] T. Medalel Masaud, P.K. Sen. Study of the implementation of STATCOM on DFIG-based wind farm connected to a power system. *IEEE PES Innovative Smart Grid Technologies (ISGT)* ; 16-20 Jan 2012; Washington, DC, pp. 1 – 7.

[5] C.Gonggui, C.Jinfu, D.Xianzhong. power flow and Dynamic optimal power flow including wind farms. *International Conference on Sustainable Power Generation and Supply (SUPERGEN '09);* 6-7 April 2009; Nanjing , pp. 1 – 6.

[6] A. S. Oshaba, E. S. Ali, Speed Control of Induction Motor Fed from Wind Turbine via Particle Swarm Optimization Based PI Controller. *Research Journal of Applied Sciences, Engineering and Technology*, Vol. 5, No. 18, May 2013, pp. 4594-4606.

[7] R.C. Duan, F. H. Wang, Z. B. Ling, Z. J. Jin. Dynamic optimal reactive power compensation control strategy in wind farms of DFIG. *IEEE Power and Energy Society General Meeting (PES),* 21-25 July 2013; Vancouver, BC, pp. 1 – 5.

[8] J.C. Munoz, C. A. Canizares. Comparative Stability Analysis of DFIG-Based Wind Farm and conventional Synchronous Generators. *IEEE Power system conference and Exposition*, 20-23 March 2011*;* Phoenix, AZ , pp. 1 - 7.

[9] Y. Zou, M. Elbuluk, Y. Sozer. A complete Modeling and simulation of Induction Generator Wind Power Systems. *IEEE Industry Applications Society Annual Meeting (IAS),* 3-7 October 2010; Houston, TX, pp. 1 – 8.

[10] D. Ming, L. Binbin, H. Pingping. Impacts of Doubly-fed Wind Turbine Generator Operation Mode on System Voltage Stability. *2nd IEEE International Symposium on Power Electronics for Distributed Generation Systems (PEDG),* 16-18 June 2010; Hefei, China, pp. 602 – 606.

[11] P.S.Chaudhari,P.P.Kulkarni,R.M.Holmukhe , Mrs.P.A.Kulkarni. TCSC for Protection of transmission Line. *3rd International Conference on Emerging Trends in Engineering and Technology (ICETET),* 19-21 Nov. 2010; Goa , pp. 356 – 361.

[12] B. Venkateswara Rao, G. V. Nagesh Kumar. Optimal Location of Thyristor Controlled Series Capacitor for reduction of Transmission Line losses using BAT Search Algorithm. *Wseas transactions on power systems*. Vol.9, 2014, pp. 459- 470.

[13] J. Vara Prasad, K. Chandra Sekhar. Optimal allocation of FACTS Controllers for Critical Loading Margin Enhancement. *International Conference on Power, Energy and Control (ICPEC)* , 6-8 Feb. 2013; Sri Rangalatchum Dindigul , pp. 86 – 91.

[14] M. A. Abdel-Moamen, N. Prasad Padhy. Power Flow Control and Transmission loss Minimization Model with TCSC for Practical power networks. *IEEE Power Engineering Society General Meeting*, 13-17 July 2003; 2; pp. 880 – 884.

[15] Ayman A. Alabduljabbar, J. V. Milanoviü. Generation Costs Reduction Throught Optimal Allocation of FACTS Devices Using Low Discrepancy Sequences. *IEEE PES Power Systems Conference and Exposition (PSCE '06),* Oct. 29 2006-Nov. 1 2006 ; Atlanta, GA , pp. 946 – 951.

[16] E. S. Ali, S. M. Abd-Elazim. TCSC Damping Controller Design Based on Bacteria Foraging Optimization Algorithm for a Multimachine Power System. *Int. J. of Electrical Power and Energy Systems* , Vol. 37, No. 1, May 2012, pp. 23-30

[17] A. Solat, A. Deihimi. a Novel scheme for Distance Protection of Series compensated Transmission lines with TCSC using Artificial Neural networks. *IEEE 20th Iranian Conference on Electrical Engineering (ICEE),* 15-17 May 2012; Tehran, Iran , pp 517 – 522.

[18] S. M. Abd-Elazim, and E. S. Ali. Synergy of Particle Swarm Optimization and Bacterial Foraging for TCSC Damping Controller Design. *Int. J. of WSEAS Transactions on Power Systems*, Vol. 8, No. 2, April 2013, pp. 74-84.

[19] S. M. Abd-Elazim, E. S. Ali. Synergy of Particle Swarm Optimization and Bacterial Foraging for TCSC Damping Controller Design. *Int. J. of WSEAS transactions on power systems*, Vol. 8 , No. 2, 2013, pp.74- 84.

[20] Y.L. Abdel Magid, M.A. Abido. Robust Coordinated Design of Excitation and TCSC Based StabilizersUsing Genetic Algorithms. *Int. J. Electr. Power Energy Syst.* Vol. 69**,** No. (2–3), 2004, pp.129–141.

[21] E. S. Ali, and S. M. Abd-Elazim. Power System Stability Enhancement via Bacteria Foraging Optimization Algorithm. *Int. Arabian J. for Science and Engineering (AJSE),* Vol. 38, No. 3, March 2013, pp. 599-611.

[22] S. Padaiyatchi , M. Daniel. OPF-based reactive power planning and voltage stability limit improvement under single line outage contingency condition throught evolutionary algorithms. *Turk J Elec Eng & Comp Sci*, Vol. 21, 2013, pp. 1092–1106.

[23] M. Khederzadeh. Application of TCSC to enhance power quality. *IEEE 42nd International Universities Power Engineering Conference (UPEC)*, 4-6 Sept. 2007; Brighton, pp. 607 – 612.

[24] H. Ghahramani, Akbar lak, M. farsadi, H. hosseini. Mitigation of SSR and LFO with a TCSC based-conventional damping controller optimized by the PSO algorithm and a fuzzy logic controller. *Turk J Elec Eng & Comp Sci*, Vol. 21, 2013, pp. 1302–1317.

[25] K.Shanmukha Sundar, H.M. Ravikumar. Enhancement of power system performance using TCSC. *In: Joint International Conference on Power System Technology and IEEE Power India Conference (POWERCON)*, 12-15 Oct. 2008; New Delhi, pp.1 – 7.

[26] F.Lakdja, F.Z.Gherbi, R.Berber, H. Boudjella. Optimal TCSC placement for optimal power flow. *Journal of Electrical Engineering*, Vol.63, 2012, pp. 316–321.

[27] F. Lakdja, D. Ould abdeslam , FZ. Gherbi. Optimal location of Thyristor controller series compensator for optimal power flows. *International Review on modelling and Simulations (I.R.E.MO.S)*, Vol.6, 2008; pp. 465–472.

[28] L. Slimani, T. Bouktir. Economic power dispatch of power systems with pollution control using artificial bee colony optimization. *Turk J Elec Eng & Comp Sci*, Vol.21, 2013, pp. 1515–1527.

[29] S.Sreejith, Sishaj P Simon , M. P. Selvan. Power Flow Analysis Incorporating Firing Angle Model Based TCSC. *5th International Conference on Industrial and Information Systems (ICIIS)*, Jul 29 - Aug 01 2010; Mangalore, India , pp. 496 – 501.

[30] R. Zarate-Mihano , A.J. Conejo , F.Milano. OPF-based security redispatching including FACTS devices. *IET Gener. Transm.Distrib*, Vol.2, 2008, pp. 821–833.

[31] F. Milano. Power System Analysis Toolbox *Documentation for PSAT version 2.0.0*, February 14, 2008.

[32] B.C.Babu, K.B.Mohanty,C.Poongothai. Wind Turbine Driven Doubly –Fed Induction Generator with Grid Disconnection. *in Magnetism, G. T. Rado and H. Suhl, Eds. New York: Academic*, Vol.3, 1963, pp. 271–350.

[33] S. Zaki Farooqui. Autonomous Wind Turbines with Doubly-Fed Induction Generators. *3rd International Conference on Energy and Environment (ICEE)*, 7-8 December 2009; Malacca, Malaysia, pp. 62 – 70.

[34] S. Sreedharan, W. Ongsakul, J. G. Singh. Maximization of instantaneous wind penetration using particle swarm optimization. *International Journal of Engineering, Science and Technology*, Vol.2, 2010, pp. 39-50.

[35] A. Al-Hinai. *Voltage collapseprediction for interconnected power systems*. Master of Sciences in Electrical Engineering. College of Engineering and Mineral Resources at west Virginia university, Morgantown, west Virginia, 2000.